Attacking the Fresh Water Crisis with Solar Power and Waste Materials:

Preparation and Electrosorption Desalination Performance of Peanut Shell Based Activated Carbon and Defect-rich MoS_2

Bole Pan Guangzhou Tianhe Foreign Language School, China

Abstract

Seawater desalination is an unavoidable path to solve the freshwater crisis. Compared with other methods, Hybrid Capacitive Deionization (HCDI) is a promising and energy-efficient method without secondary pollution. In this study, molybdenum disulfide (MoS_2) was prepared using hydrothermal methods, and defects were introduced through thermal treatments. Activated carbon was prepared based on the waste shell of peanut, which is a crop of drought tolerance and great yield. The synthesized materials were characterized using X-ray diffraction (XRD), Raman spectra, scanning electron microscope (SEM), transmission electron microscope (TEM), energy dispersive spectrometer (EDS), electrochemical workstation and BET method. The HDCI study was performed on the desalination performance of 1000mg/L NaCl solution under a voltage of 1.2V with defect-rich MoS_2 as the cathode and peanut-shell based activated carbon as the anode. The hybrid electrodes exhibited an electrosorption capacity of 8.98mg/g in 60 minutes. Moreover, a solar-powered, automated, portable machine was assembled incorporating the obtained electrodes and successfully processed sea water from South China Sea (TDS=17g/L) to fresh water (TDS=0.2g/L) within nine cycles of adsorption-desorption processes, validating the possibility of using solar power as the sole power source for HDCI is proven during tests and implicating the application prospects of the study for portable seawater desalination in arid coastal and island regions worldwide.

Keywords: Capacitive deionization, peanut shell, activated carbon, MoS_2, defect, solar power

1. Introduction

Water scarcity has become increasingly perturbing nowadays, posing threats to the development of society. Despite that 71% of the planet's surface is covered with water, only 2.5–2.75% is fresh water, 1.75–2% as frozen in glaciers, ice and snow, 0.5–0.75% as fresh groundwater and soil moisture [1]. A meager portion (less than 0.01%) in rivers, lakes, and swamps is safe and attainable for humans [2]. Four billion people are facing severe water scarcity,

accounting for more than 50% of the global population [3]. Saline water in oceans, seas and saline groundwater make up about 97% of the total amount of water; so it is evident that seawater desalination is an inevitable path to tackle the water crisis. Traditional desalination methods include distillation, reverse osmosis, electrodialysis, etc. Of all, RO, accounting for 67.5% of the industry, is the biggest desalination process internationally [4]. However, seawater desalination was not universally adopted to produce drinking water at the commercial scale for its high capital and energy costs [5-7]. Electrosorption Deionization, or Hybrid Capacitive deionization (HCDI), is normally used in brackish water desalination but not seawater desalination [8]. It is of great interest due to its high energy efficiency, environmental friendliness, and low-cost operation. The key for its application on seawater desalination is the development of electrode materials of large specific surface area, conductivity, and high capacitance.

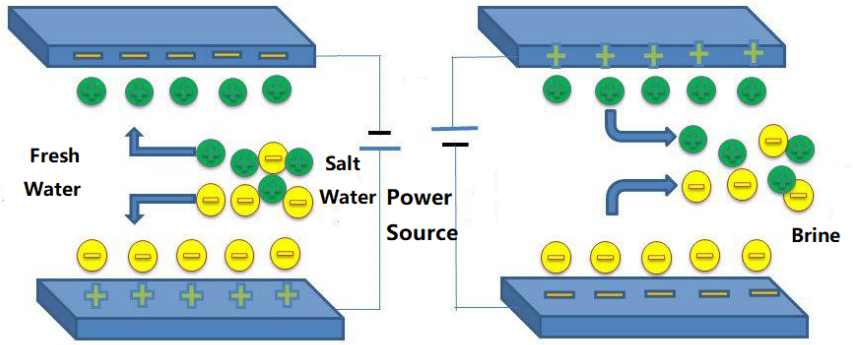

Fig.1. Principle of Hybrid Capacitive Deionization

Activated carbon (AC) is the conventional material for the preparation of electrodes for CDI application due to its high surface and good electronic conductivity, stability, and matured production techniques [9-11]. However, as the cost of producing activated carbon increased, recycling of biomass wastes for the synthesis of activated carbon is becoming attractive both economically and environmentally [12]. Previous researches have included the preparation of AC from crop straw, corn cobs, etc. [13] [14]. Peanut is a crop with drought tolerance capability and worldwide distribution. The annual yield of peanut in the world is 25.68 million tons. The world's peanut growing areas are mainly in Asia, Africa, and America. Among them, the planting area of peanut in Asia is 13.47 million hm^2, accounting for 63.4% of the total planting area in the world; Africa is 6.54 million hm^2, accounting for 30.8%; America is 1.16 million hm^2, accounting for 5.5% [15]. Using peanut shell waste to prepare activated carbon can not only be environmentally friendly but can also better serves the arid regions worldwide.

Moreover, to bring faster access of sodium ions into the electrode, 2D materials might be more suitable for being the CDI electrode material due to their ultrahigh surface-to-volume ratio. Molybdenum disulfide (MoS_2) is a typical layered transition-metal dichalcogenide, which consists of two hexagonal sheets of sulfur atoms and one intermediate hexagonal sheet of molybdenum atoms. The 2D MoS_2 possesses a huge specific surface area, providing an ideal platform for physical and chemical reactions. Recent studies indicated that MoS_2 exhibited outstanding performances and superior abilities for various dyes and heavy metals removal due to structure suitable for ion intercalation [16-18]. Also, defects have been proven to enhance the performance of MoS_2 by lowering the impedance, making it easier for ions to approach the surface of the electrode [19].

Also it is evident that the intensity of regional solar irradiation is positively correlated with the severity of local water scarcity. It would be an excellent solution to turn this potent source of vaporization into the energy source of desalination.

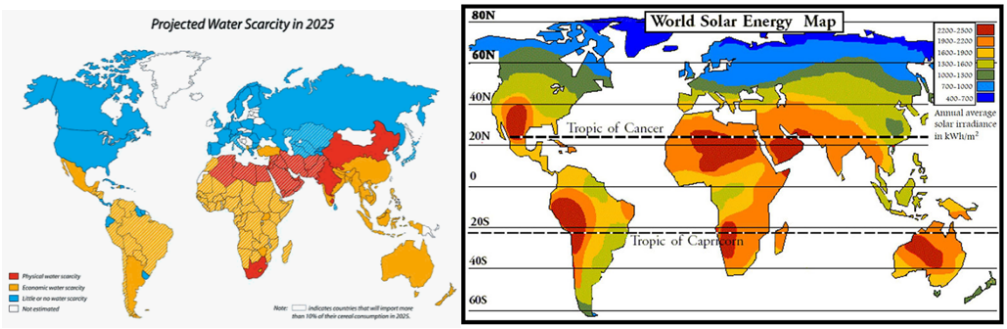

Fig.2. Global water scarcity and world solar energy map (source: ResearchGate.net)

This research aims to fabricate AC from recycled peanut shell wastes and to introduce defects to MoS_2 to enhance performance for capacitive desalination. The study also discusses the possibility of using solar power for desalination.

2. Experimental

2.1. Materials and reagents

All the reagents used in these experiments were of analytical grade. Sodium molybdate (Na_2MoO_4), thiourea (CN_2H_4S), sodium chloride (NaCl), potassium hydroxide (KOH), Acetylene black, carbamide (CH_4N_2O) and N-Methyl pyrrolidone (C_5H_9NO) used in this study were purchased from the Damao Chemical Reagent Co., Ltd. (Tianjin, China). Polyvinylidene difluoride（PVDF） was purchased from Arkema Kynar Co., Ltd. (France). All solutions were

prepared with ultrapure water from a Milli-O System.

2.2. Methods

2.2.1 Preparation of peanut shell based activated carbon

Activated carbon was prepared based on peanut shells. Peanut shells were washed, torn into pieces and dried under sunlight for 48 hours. The pretreated shells were then put into crucibles and then into a SX2-4-10A (Huyueming Co. Ltd. Shanghai, China) muffle furnace, and were carbonized at 450 ℃ for 2 hours. The samples were washed and dried at 60 ℃ for 8 hours to obtain peanut shells based carbon materials. The materials were then ground into powder and mixed with potassium hydroxide (KOH), carbamide (CH_4N_2O) in a weight ratio of 1:2:1. The mixed powder was stirred and soaked in deionized water for 24 hours. After washing and drying, it is calcined in nitrogen flow for 3 hours at 750 ℃. The product is washed with hydrochloric acid solution and deionized water and dried. Peanut shell-based activated carbon obtained in this study is named P-AC for brevity.

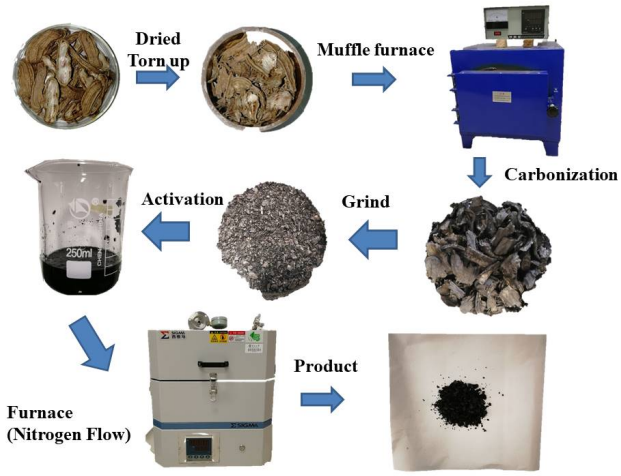

Fig.3. The preparation process of peanut shell based activated carbon

2.2.2 Preparation of defect-rich molybdenum disulfide

Molybdenum disulfide was synthesized by a one-step hydrothermal method. 0.5 g sodium molybdate ($Na_2MoO_4.2H_2O$) and 0.7 g thiourea (CN_2H_4S) were dissolved in 90 mL deionized water. The solution was vigorously stirred for 30 minutes to form a homogeneous solution and ultrasonicated for 15 minutes. Then the mixture was transferred into a 100ml Teflon-lined stainless steel autoclave. It was kept at 180 ℃ for 24 h. After cooling down, it is filtered and washed twice with deionized water and ethanol and dried at 60 ℃ for 8 h to obtain molybdenum

disulfide. The sample was subjected to thermal treatment at 290℃ for 2h in the muffle furnace to introduce defect, followed by washing the as-prepared sample with deionized water for the removal of oxides. The thermally treated sample was named as D-MoS_2 in this study.

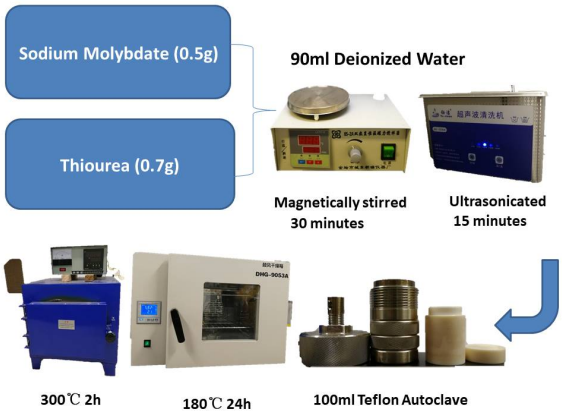

Fig.4. The preparation process of defect-rich MoS_2

2.2.3 Preparation of electrodes

P-AC electrode was prepared by mixing pretreated P-AC powder, Polyvinylidene difluoride （PVDF）and Acetylene black in a weight ratio of 8:1:1. N-methyl pyrrolidone was added to the mixed powder and the mixture was magnetically stirred for 3 hours and then ultra-sonicated for 1 hour at room temperature to form a homogeneous solution. The mixture was dried in the furnace at 60 ℃ till thickened and then applied to 6 cm * 8 cm nickel foams. The P-AC electrodes were obtained by drying for 8 hours before being pressed by a press machine and dried for another 4 hours. D-MoS_2 electrodes were prepared following the same method of P-AC electrodes, only replacing P-AC with D-MoS_2. To eliminate the ions introduced during preparation, all prepared electrodes were washed with deionized water and then dried before desalination experiments.

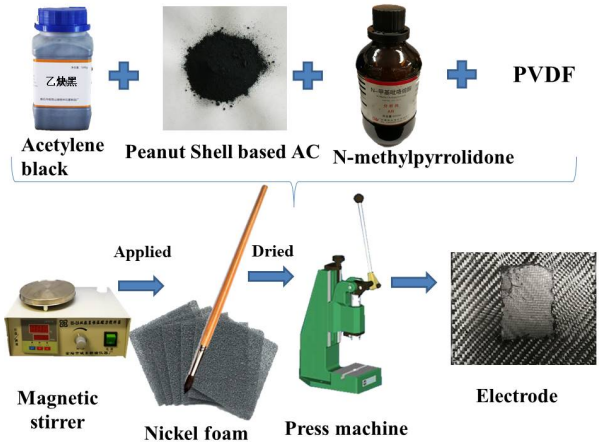

Fig.5. The preparation process of electrodes

2.3 Characterization

The morphologies of samples were characterized by a scanning electron microscope (SEM, JSM-6701F Quanta 400FEG) and X-ray energy dispersive spectroscopy (EDS). The Brunauer–Emmett–Teller (BET) surface area of electrodes was performed on the 3H-2000 automatic specific surface area analyzer with nitrogen adsorption/desorption at 77 K. The structure and composition of the samples were characterized by powder X-ray diffraction (XRD, D-MAX 2200 VPC) and Raman spectra (Renishaw inVia Raman Microscope). Cyclic voltammetry (CV) and Electronic Impendence Spectra (EIS) were carried out in a three-electrode cell with the electrolyte of 0.5M Na_2SO_4 solution using a CHI7601 electrochemical workstation.

2.4 Electrosorption experiments

The electrosorption performances of the electrodes were tested in a self-made HCDI system, which was schematically represented in Figure. 6 Two electrodes of nickel foams coated with P-AC, regular AC, D-MoS_2 or regular MoS_2 composite were placed in a customized cell as electrodes. There was 1 mm of the distance between the positive and negative electrode. A potential of 1.2 V was applied to the electrode by either a battery or a solar panel under sunlight irradiation. During the electrosorption desalination experiment, 150 mL of NaCl solution with a concentration of 1000mg/L continuously flow through the system by a peristaltic pump. A beaker was used as a buffer, and an electrical conductivity meter (EC meter) was applied to determine the electrical conductivity of the solution. Electrical conductivity employed as the proxy for NaCl concentration in this experiment. The electrosorption capacity of NaCl of the electrodes was calculated according to Equation (1).

$$\mathbf{p} = \frac{(\boldsymbol{e_0}-\boldsymbol{e}) \times \boldsymbol{V}}{\boldsymbol{m}} \qquad \textit{Equation (1)}$$

Where e_0 and e are the electrical conductivity of the solution at the initial time and time t, respectively, V is the volume of the electrolyte (L); m is the mass of active materials on cathode and anode (g).

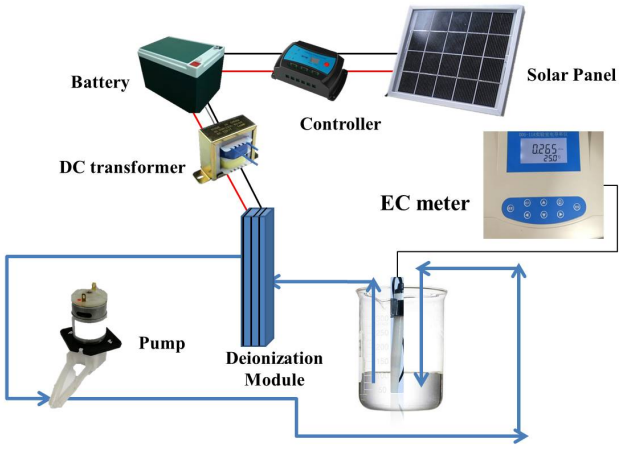

Fig.6. Set up for electrosorption experiments with a solar power source

3. Results and Discussions

3.1 Structure and Morphology of Activated Carbon

XRD was adopted to gain insights into the structures of P-AC and AC. As indicated in Fig.7. (a), two strong and broad diffraction peaks at 2θ of 24.7° and 43.6°corresponds to the (002) planes and (100) planes of the graphitic carbon (JCPDS No. 75-1621) [20]. The patterns of P-AC and AC are generally similar, suggesting both of which are synthesized of ordered structure. The appearance of a few unidentified peaks might be ascribed to the porous structure on the plate surface. The Raman spectra of AC and P-AC, as shown in Fig.7(b), were dominated by the relatively sharp first order graphitic G (near 1580 cm^{-1}) and D (near 1340 cm^{-1}) bands, featuring the graphitic sp2 sites [21].

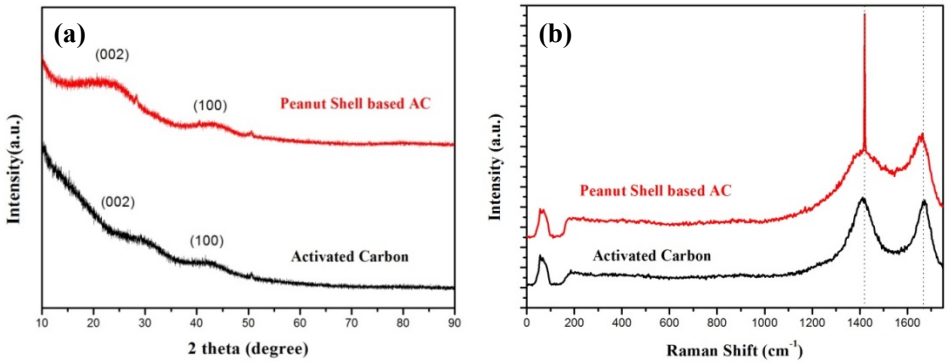

Fig.7. XRD pattern (a) and Raman spectra (b) of P-AC and AC

The morphology of AC and P-AC were investigated using SEM. As shown in Figure, images of AC (Figure 8 (a-b)) revealed its porous structure. However, P-AC's pores have a larger width,

as illustrated in Figure 8 (c-d). In image (d), 17 holes with a diameter greater than 1μm are visible, compared to 8 in image (b) of the identical scale. The large width of P-AC's pores is attributed to the nature of biomass materials.

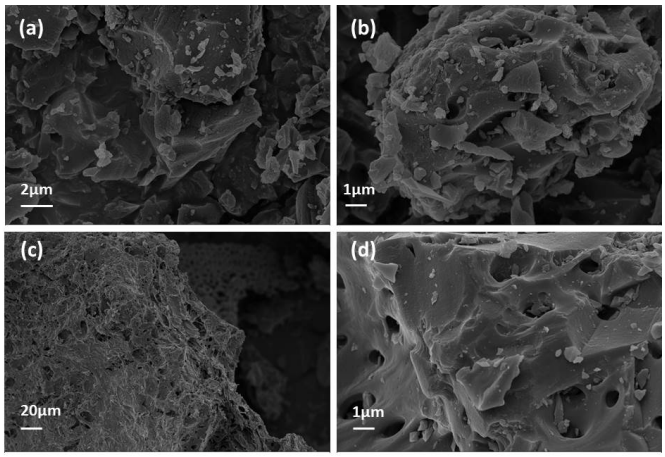

Fig.8. SEM images of AC (a) (b) and P-AC (c) (d)

Table 1 shows the BET surface area, pore volume, and diameter of AC and P-AC. It can be seen that the BET surface area of AC is almost 200 times that of P-AC, and the pore volume of AC also exceeds P-AC's by a great margin. Nonetheless, P-AC revealed an average pore width of 6 times greater than AC's. It is generally believed for electrode materials that the larger the specific surface area of is, the higher the electrosorption capacity will be. However, experiments show that capacities are also related to sizes of pores, surface functional groups, electrolytes, and many other factors. Pores of various sizes have different adsorption effects on different aqueous solvents. In theory, only pores with a size of 0.5nm and above can absorb ions electrochemically. The adsorption speed is different for different pore sizes, the larger the pores, the faster the electrochemical adsorption speed [22] [23]. In short, P-AC falls short in criteria of surface area and pore volume but stands out in pore width. It has its advantages, but its shortcomings are to be dealt with in further researches.

Table 1 BET surface area, pore volume, and diameter of AC and P-AC

	AC	P-AC
BET Surface Area	1,557.12 m^2/g	78.86 m^2/g
D-H Adsorption average pore width	3.03 nm	18.32 nm
Total pore volume of pores	0.74 cm^3/g	0.032 cm^3/g

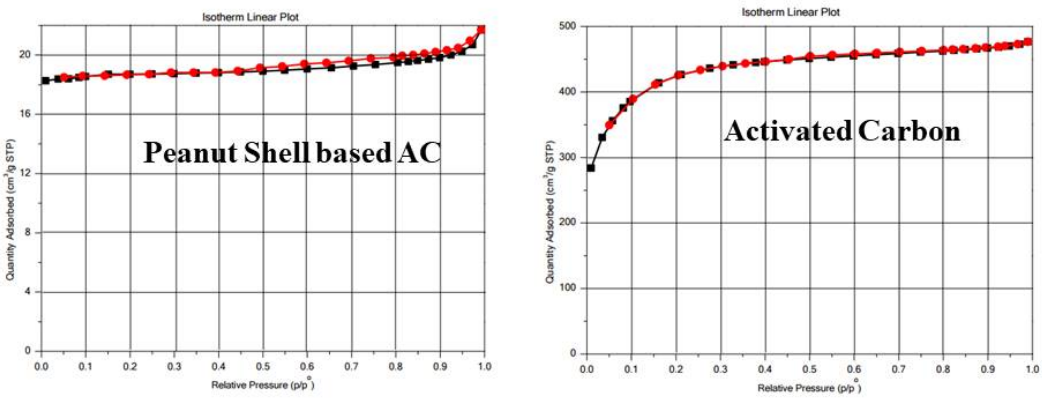

Fig.9. Adsorption/desorption isotherms of AC and P-AC

3.2 Structure and Morphology of Molybdenum Disulfide

The XRD pattern of MoS_2 and D-MoS_2 is illustrated in Fig.10 (a). The distinct diffraction peaks at 2θ of 13.55°, 32.43°, 35.52°, 57.30° correspond to the primary diffractions of (002), (100), (103) and (110) planes of MoS_2, agreeing with a hexagonal structure of MoS_2 (JCPDS: 37-1492). This indicated the successful synthesis of MoS_2 with excellent crystallinity. The pattern of D-MoS_2 showed numerous unidentified peaks emerging in the entire range, indicating defects in the crystal plane. This proved the successful introduction of defects on MoS_2 after thermal treatment for 2 hours at 290℃. Raman spectra of molybdenum disulfide before and after thermal treatment are displayed in Fig.10 (b). Two characteristic peaks at 200cm^{-1} and 409.4 cm^{-1} of molybdenum disulfide were observed, which are in line with the in-plane displacement in Mo and S atoms (E2g1) and out-plane symmetric displacement of S atoms along the c-axis (A1g), respectively. [24]

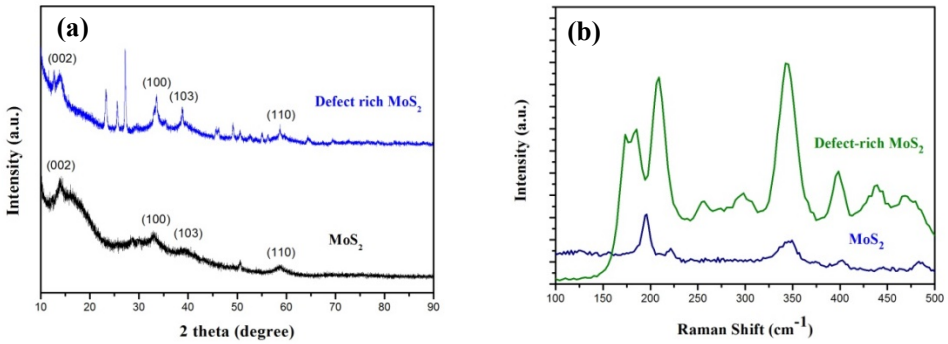

Fig.10. XRD pattern (a) and Raman spectra (b) of MoS_2 and D-MoS_2

The chemical composition of the D-MoS_2 was further confirmed by EDS analysis. Fig. 11 suggests that the MoS_2 microspheres are composed of mainly Mo and S, proving the purity of the

sample after thermal treatment. The element of Cu is the result of the supporting basement.

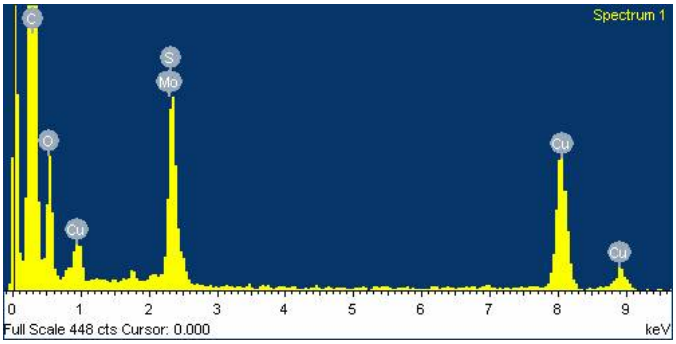

Fig.11. EDS spectra of D-MoS_2

Fig.12. shows the SEM images of MoS_2 (a) (b) and D-MoS_2 (c) (d). It can be seen that MoS_2 is in spheres with uniform sizes around 5μm in diameter, and the spheres are linked together to form larger objects of approximately 10-15μm in diameter. After being thermally treated at 300 °C, D-MoS_2 presented a similar morphology, since defects are not visible at the scale.

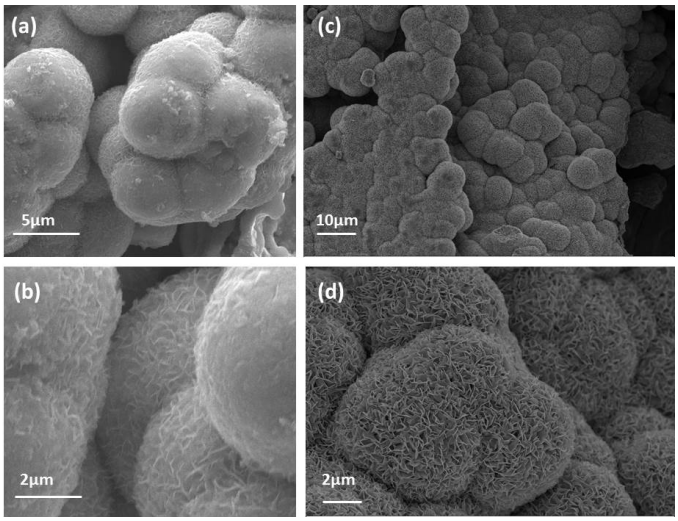

Fig.12. SEM images of MoS_2 (a) (b) and D-MoS_2 (c) (d)

The TEM images of MoS_2 are shown in Fig. 13(a–b). The good transparency of these obtained nanosheets to visible light indicated the thin thickness of MoS_2, crediting the hydrothermal method. It is also evident that the nanosheets are with a layered structure, resulting in its large specific surface area.

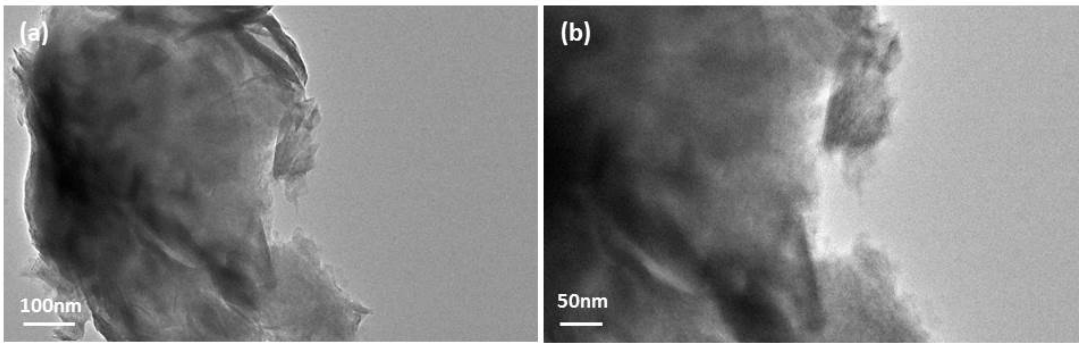

Fig.13. TEM images of MoS_2

On the adsorption/desorption isotherms of Figure.14., the specific surface area, pore volume and the size of MoS_2 and D - MoS_2 were computed and given in Table 2. The specific surface area of MoS_2 increased from 13.3386 m^2/g to 16.3391 m^2/g after modification treatment. Correspondingly, an increase of total pore volume and average pore size is observed on D-MoS2. The data revealed that the introduction of defects changed the morphology of MoS_2.

Table 2 BET surface area, pore volume, and diameter of MoS_2 and D-MoS_2

	MoS_2	D-MoS_2
BET Surface Area	13.34 m^2/g	16.34 m^2/g
D-H Adsorption average pore width	15.25 nm	27.51 nm
Total pore volume of pores	0.041 cm^3/g	0.090 cm^3/g

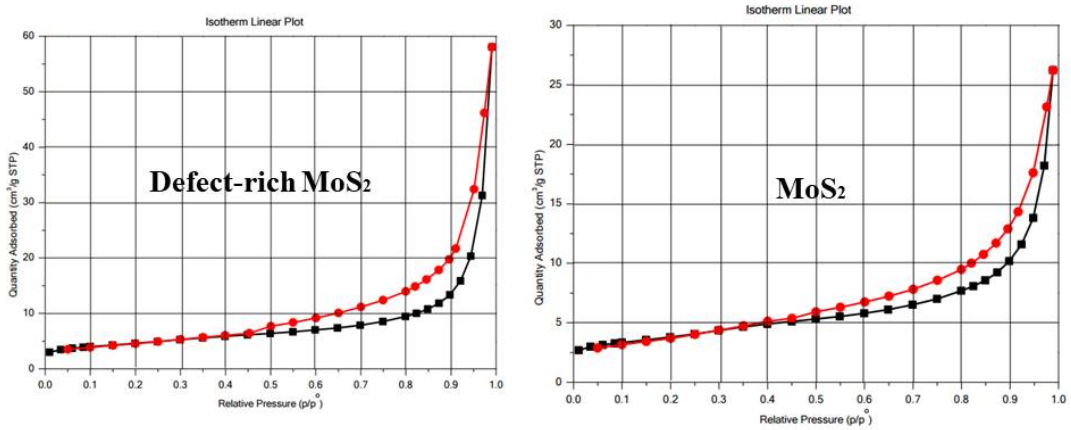

Fig.14. Adsorption/desorption isotherms of MoS_2 and D-MoS_2

3.3 Electrochemical Measurements

The electrochemical measurements were carried out Ivium Stat electrochemical workstation (Ivium Technologies BV, Netherlands). Electrochemical Impedance Spectroscopy is tested under open-circuit conditions, with a scanning frequency of 10 000 Hz-0.01 Hz.

From Figure.15., it can be told that curves AC and P-AC are different from the typical Nyquist curves, which consists of three parts of different frequencies. This variation can be ascribed to the mixed composition and rough structures of the surface of the electrodes. In low-frequency region, AC displayed better capacitance performance. It can be seen from Figure.15. that the AC curve has a large slope than P-AC curve and closer to being vertical. The closer the curve is to vertical, the easier it is for the electrolyte to approach the electrodes' surface. Therefore, electrolyte ions can approach the surface of AC electrode more easily, enhancing its performances. However, the x-intercept for P-AC is smaller than that of AC. As a result, there is less resistance for P-AC than AC in high-frequency region, as the x-axis intercept is impedance in the solution [25].

Similarly, as the curve of defect-rich MoS_2 possesses a small x-intercept and a steeper slope, it can be concluded that defect-rich MoS_2 exhibited superior performances in both regions of high and low frequencies.

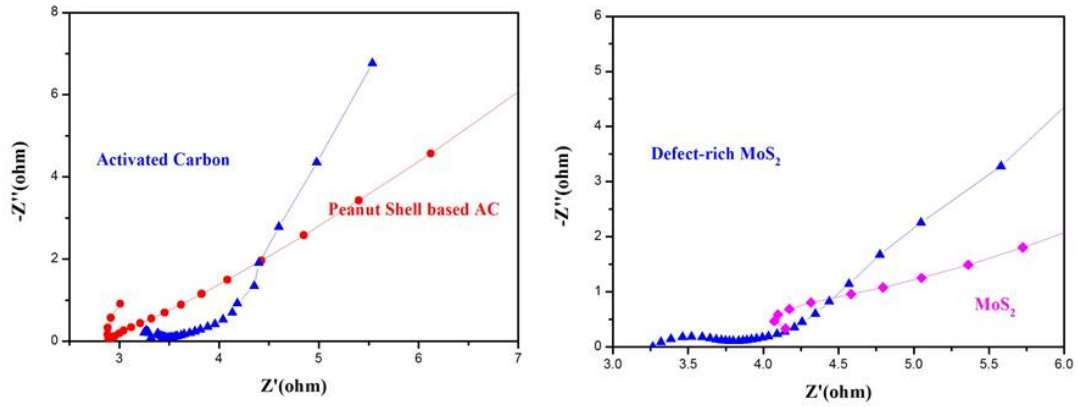

Fig.15. EIS spectra of AC, P-AC, MoS_2, and D-MoS_2

The Cyclical voltammetry measurements of the MoS_2, D-MoS_2, AC and P-AC electrodes were obtained with a conventional three-electrode. As shown in Figure.16., no sharp redox peaks are visible for all of the four curves, which is in good agreement with the typical Electric Double Layer capacitance of the electrodes. Nevertheless, the capacitance of P-AC is significantly smaller than that of AC, which is in line with the BET analysis. P-AC's relatively small surface area agrees with its lower capacitance. This ought to be addressed through grinding the material thoroughly and upgrading ways of activation. The capacitance of D-MoS_2 is similar to that of MoS_2.

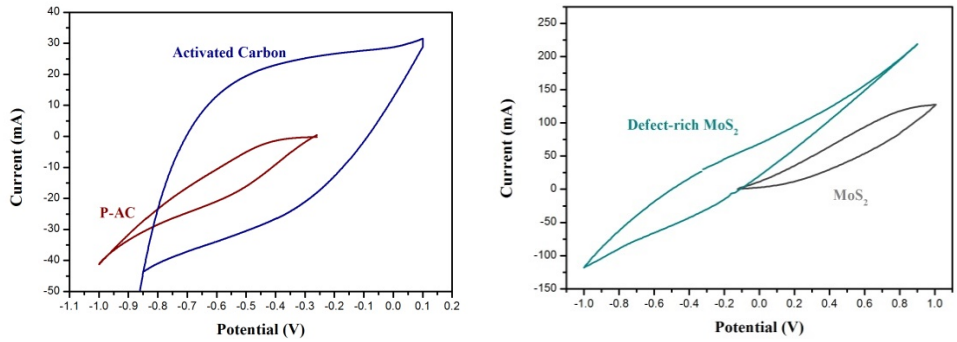

Fig.16. CV curves of AC, P-AC, MoS_2, and D-MoS_2

3.4 Electrosorption Desalination Performances

Saline water was stimulated using NaCl solution in the experiments. Because of convenience, Electrical Conductivity was chosen as the proxy for NaCl concentration. Various concentrations of NaCl solutions were prepared and each solution's electrical conductivity was measured using an EC meter. Figure 17 displayed a good linear correlation (R^2=0.999) between the concentration (C) and conductivity (Ec):

$$Ec = 2.01315\ C + 45.07$$

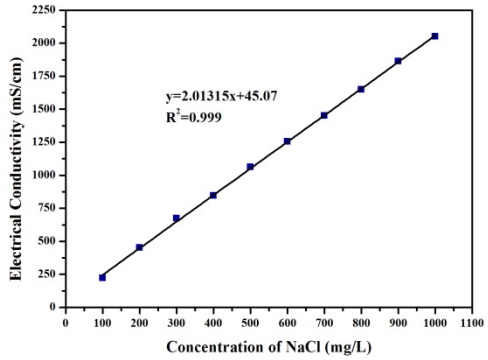

Fig.17. Correlation between NaCl concentration and electrical conductivity

Previous researches revealed that the electrosorption capability is in part in a positive correlation to the potential applied on the electrodes. However, too high a potential would trigger redox reactions. The ideal potential is in between 1.2-1.5V. In the study, a potential of 1.2V is applied to the pump and the electrodes by a DC transformer and a 12V battery charged up using solar energy. NaCl solution of 1000 mg/L with electrical conductivity of 2050 μS/cm flowed through the system for one hour. Electrosorption desalination performances of combinations of P-AC/P-AC and P-AC/D-MoS_2 are shown in Figure 18. Electrical conductivity decreased at steady rates over the course, and P-AC/P-AC electrodes displayed a removal rate of 28.7%, while

P-AC/D-MoS_2 of 35%. The latter's performance exceeds the former.

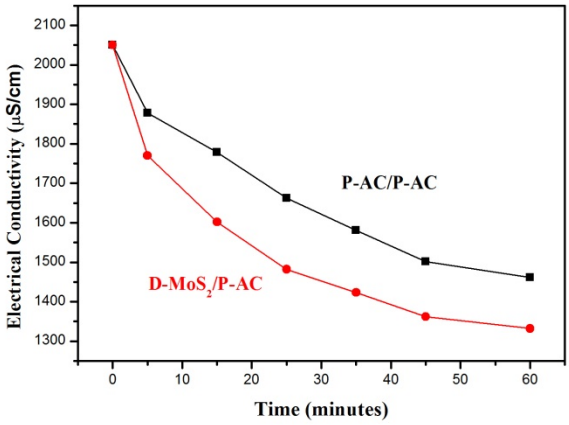

Fig.18. Capacitive deionization performance of P-AC electrodes and P-AC/D-MoS_2 electrodes

Experiments with the various initial concentrations of NaCl were also conducted. After 60 minutes of desalination, the electrosorption capacity was calculated for each run employing the Equation (1) above. As it can be seen from Figure.19, as initial concentration increases, the electrosorption capacity elevates also. At 1000mg/L of initial NaCl, the capacities for P-AC/P-AC and P-AC/D-MoS_2 are 7.92mg/g and 8.98mg/g, respectively. The contrast of the two suggested the superiority of P-AC/D-MoS_2 electrodes.

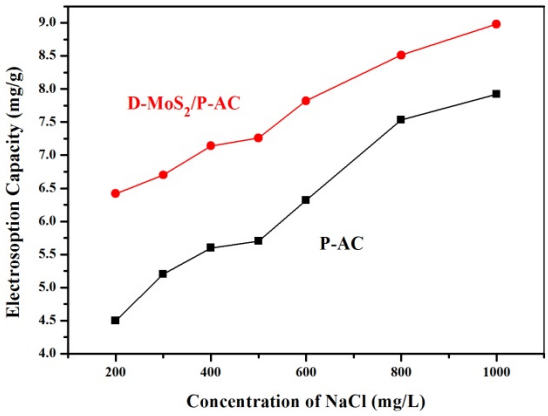

Fig.19. Electrosorption Capacity of the electrodes and the initial concentration of NaCl

The renewability of the electrodes is one of the distinctive attributes of capacitive deionization. After reaching the electrosorption limits, electrodes can be reused by reversing the connection of the battery, which causes desorption of ions. NaCl solution of 300mg/L was used to study the absorption-desorption capabilities. It is illustrated in Figure.20 that the electrosorption capacity didn't show decrease after 4 cycles. It can also be learned that D-MoS_2/P-AC electrodes possess not only a higher capacity but also a short cycle period for deionization.

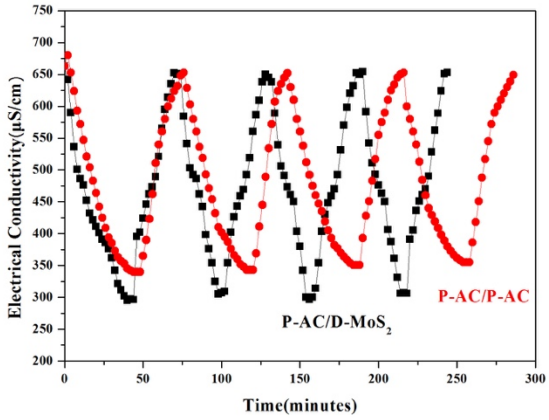

Fig.20. Cyclic absorption/desorption performance of P-AC electrodes and P-AC/D-MoS_2 electrodes

3.5 Application

To confirm the possibility of using solar energy as the sole power source for electrosorption desalination and further test the synthesized materials' performances, field tests are conducted using an experimental set up as shown in Figure.21 and Figure.22. The electrodes were placed in a container with cathode coated with peanut shell based activated carbon and anode of activated carbon fiber. The time need for the electrodes to reach saturation was pre-tested and timed switches are used to help realize the automation of the adsorption/desorption process.

The field tests were carried out using real seawater obtained from the South China Sea (TDS=17.0g/L). As shown in Figure.23, after nine cycles of adsorption/desorption processes, TDS decreased from 17.0g/L to 0.2g/L, while the electrical conductivity decreased from 32.0 mS/cm to 0.4mS/cm, both meeting the standards of fresh water, proving the possibility and immense application prospects of this research.

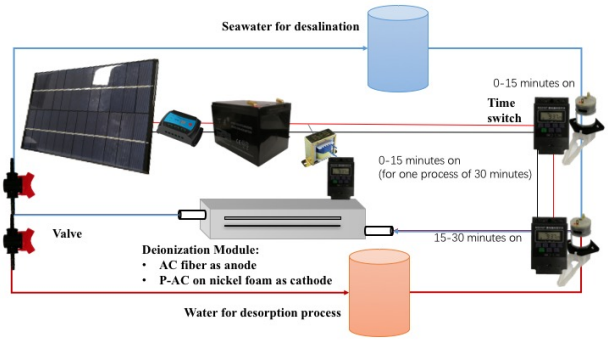

Fig.21. Experimental setup of field tests

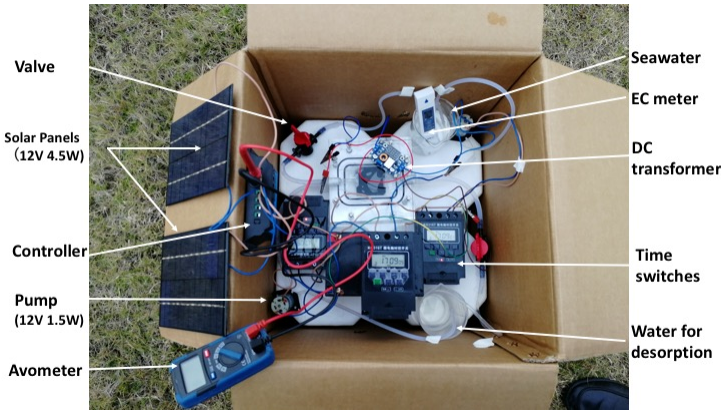

Fig.22. Illustrated graph of the experimental set up

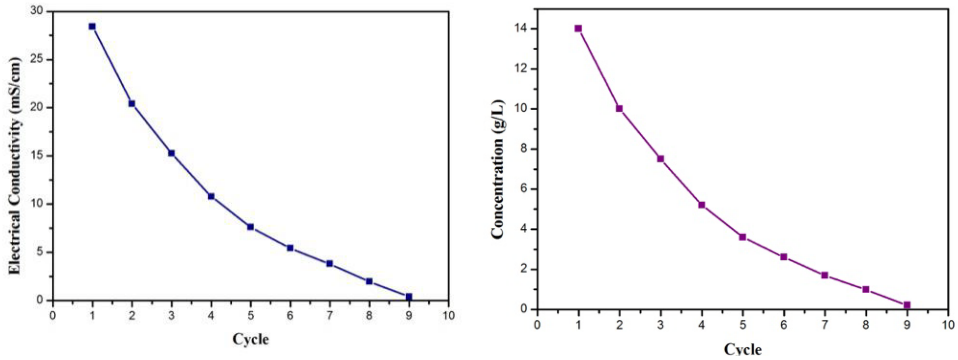

Fig.23. Changes in electrical conductivity and TDS of the sample sea water of field tests

3.6 Discussions of Practicality

According to previous researches [26-28], a comparison of the electrosorption capacity of different electrode materials was listed out in Table 3 below. It can be seen that P-AC electrodes, although they have an inferior surface area to AC, showed more electrosorption capacity than AC electrodes, indicating the superiority of biomass materials and its immense potential.

Table 3 Comparison of electrosorption capacity

Materials	Initial concentration of NaCl	Voltage	Electrosorption Capacity
AC/AC	1000	1.2V	7.12mg/g
AC/carbon nanotubes	150	1.2V	7.29mg/g
ce-MoS_2	400	1.2V	8.81mg/g
P-AC/P-AC	1000	1.2V	7.92mg/g
P-AC/D-MoS_2	1000	1.2V	8.98mg/g

Reverse Osmosis accounts for up to 67.5% of the desalination industry. As electrosorption

(capacitive deionization) starts to gain popularity, it is essential to contrast the two methods to determine their different advantages. Table 4 shows the comparison. [29] Accordingly, HDCI exceeds its competitor in various degrees, including water requirements, process flow, and percentage yield. The water quality of HCDI is below that of RO, and that is the reason for continued researches in this field. The investment and cost of the two are listed out in Table 5. The initial investment for HCDI excesses RO's, but HDCI surpasses the latter in required space, annual cost, and marginal cost. The difference between the investments can be offset in approximated 3 years.

Table 4 Comparison of RO and HCDI in water requirements, process flow percentage yield, and water quality

Methods	HCDI	Reverse Osmosis	Results
Water requirements	COD <60mg/L	COD <30mg/L	HCDI has a less strict demand
Process Flow	➢ Filtration ➢ HCDI Module	➢ Filtration ➢ Ultrafiltration ➢ RO	HCDI's process is simpler
Percentage Yield	95%	75%	HCDI yields more water
Water quality	TDS below 800 mg/L。	TDS below 150 mg/L。	RO can produce better water quality

Table 5 Comparison of RO and HCDI in investment and cost

Methods	HCDI	RO	Results
Investment on building a 400m^3 facility	\$4 million	\$3 million	RO requires less investment
Space	2400 m^2	3200 m^2	HCDI requires a small space
Annual cost	\$0.85 million	\$1.18 million	HCDI has a lower cost
Cost per water unit	\$0.35	\$0.52	HCDI has a lower marginal cost

3.7 Limitations

This research has the following limitations. First, to improve the efficiency of the adsorption process, the obtained P-AC's surface area needs to be enlarged. Further modifications, changing of

activation agents or grinding before activation can all be explored as ways to increase the surface area. Second, the synthesizing process involved several non-biodegradable materials, like the binder PVDF. In further research, these materials can be replaced with their biodegradable counterparts, like a natural binder. Third, the MoS_2, a metal disulfide used in this research, may not be obtainable worldwide. In the field tests, the electrode combination of P-AC and AC fiber has proven the capability of using all-carbon electrodes Further research can consider to continue to enhance the performance of activated carbon in electrosorption.

4. Conclusion

In this work, a peanut shell was used to prepare activated carbon, while defects were introduced to MoS_2 through thermal treatment. CDI performances were tested to obtain an electrosorption capacity of 7.92 mg/g and 8.98mg/g for P-AC/P-AC and P-AC/D-MoS_2, respectively. Characterization result revealed the enhanced performances of D-MoS_2 origin from the lowering of impedance due to the introduction of defects, while P-AC's were ascribed to enlarged pores width. P-AC's surface area can be further improved by upgrading ways of activation. As the possibility of using solar power for HCDI was validated during experiments, the study has prospects of applied in resolving water crisis in arid coastal and island regions worldwide.

Acknowledgments

This project is supported financially by the Talent Program of Children & Youth Science Center (CYSC), affiliated to the China Association for Science and Technology (CAST). The author sincerely appreciates the guidance and support of Prof. Yexiang Tong from Sun Yat-sen University and Prof. Yongzhang Pan from Jinan University.

References

[1] 钱易. "环境保护与持续发展." *科学中国人* 6(1995):7-11.

[2] Central Intelligence Agency. "CIA – The world facctbook". Archived from the original on 1 February 2010. (2010)

[3] Mekonnen, M. M., and A. Y. Hoekstra. "Four billion people facing severe water scarcity." *Science Advances* 2.2(2016):e1500323-e1500323.

[4] 王世昌, 周清, and 王志. "海水淡化与反渗透技术的发展形势." *膜科学与技术* 23.4(2003):000162-171.

[5] Service, R. F. "Desalination freshens up." *Science* 313.5790(2006):1088.

[6] Shannon, M. A., et al. "Science and technology for water purification in the coming decades. " *Nature* 452.7185(2008):301-10.

[7]Schiermeier, Quirin. "Water: Purification with a pinch of salt." *Nature*452.7185(2008):260-261.

[8] Li, Chennan , Y. Goswami , and E. Stefanakos . "Solar assisted sea water desalination: A review." *Renewable and Sustainable Energy Reviews* 19(2013):136-163.

[9] Santoro, C, et al. "Supercapacitive microbial desalination cells: New class of power generating devices for reduction of salinity content. " *Applied Energy* 208(2017):25-36.

[10] Zornitta, Rafael L., et al. "High-performance activated carbon from polyaniline for capacitive deionization." *Carbon* 123(2017).

[11] Huang, Wei, et al. "Desalination by capacitive deionization process using nitric acid-modified activated carbon as the electrodes." *Desalination*340.1(2014):67-72.

[12] Tay, T, S. Ucar, and S. Karagöz. "Preparation and characterization of activated carbon from waste biomass. " *Journal of Hazardous Materials*165.1(2009):481-485.

[13] 邢宝林等. "玉米芯活性炭的制备及其电化学性能研究." *材料导报* 29.6(2015):45-48.

[14] Zheng, Qiu Sheng, L. I. Long, and H. U. Xue-Yu. "Research Progress in Activated Carbon Preparation from Crop Straw." *Journal of Cellulose Science & Technology* (2010).

[15] Ahmad, M, et al. "Biochar as a sorbent for contaminant management in soil and water: a review. " *Chemosphere* 99.3(2014):19-33.

[16] Ding, Shuang Shuang, et al. "Dual role of monolayer MoS2 in enhanced photocatalytic performance of hybrid MoS2/SnO2 nanocomposite." *Journal of Applied Physics* 119.20(2016):1239176.

[17] Jia, F., X. Zhang, and S. Song. "AFM study on the adsorption of Hg2+ on natural molybdenum disulfide in aqueous solutions. " *Physical Chemistry Chemical Physics Pccp* 19.5(2017).

[18] Jia, Feifei, et al. "Two-Dimensional Molybdenum Disulfide as a Superb Adsorbent for Removing Hg2+ from Water." *Acs Sustainable Chemistry & Engineering* 5.8(2017).

[19] Jia, Feifei, et al. "Defect-rich molybdenum disulfide as electrode for enhanced capacitive deionization from water." *Desalination* 446 (2018): 21-30

[20] Hou, Jianhua, et al. "Hierarchical porous nitrogen-doped carbon nanosheets derived from silk

for ultrahigh-capacity battery anodes and supercapacitors." *ACS nano* 9.3 (2015): 2556-2564.

[21] Ghosh, Anupama, et al. "CO2 Sensing by in-situ Raman spectroscopy using activated carbon generated from mesocarp of babassu coconut." *Vibrational Spectroscopy* 98 (2018): 111-118.

[22] Qu, Deyang, and Hang Shi. "Studies of activated carbons used in double-layer capacitors." *Journal of Power Sources* 74.1 (1998): 99-107.

[23] Shi, Hang. "Activated carbons and double layer capacitance." *Electrochimica Acta* 41.10 (1996): 1633-1639.

[24] Lee, Changgu, et al. "Anomalous lattice vibrations of single-and few-layer MoS2." *ACS nano* 4.5 (2010): 2695-2700.

[25] Song, Hyun-Kon, et al. "The effect of pore size distribution on the frequency dispersion of porous electrodes." *Electrochimica Acta* 45.14 (2000): 2241-2257.

[26] 毕慧芝, and 田秉晖. "电吸附活性炭电极制备及电吸附特性." *环境工程学报* 9.4(2015):1606-1612.

[27] 马力等. "改性活性炭/碳纳米管复合电极脱盐性能研究." *应用化工* 4(2018).

[28] Xing, Fei, et al. "Chemically exfoliated MoS2 for capacitive deionization of saline water." *Nano Energy* 31 (2017): 590-595.

[29] 黄政. "电吸附技术与反渗透技术在市政污水回用处理中的应用." *大氮肥* 35.4(2012):256-258.